Indian Journal of Pure & Applied Physics
Vol. 63, October 2025, pp. 892-900
DOI: 10.56042/ijpap.v63i10.14328

Effect of Nickel Doping and Decoration on Electronic Properties of Monolayer Molybdenum Disulfide

Hadeel Mahir Awad[a], Issa Z Hassan[b*], & Sufyan M Nayif[a]

[a]Kirkuk Education Directorate, Kirkuk 36 001, Iraq

[b]Department of Physics, College of Education for Pure Sciences, University of Kirkuk 36 001, Iraq

Received: 11th October 2024; accepted: 12th September 2025

Doping is an effective method to manipulate the electronic properties of semiconductors. Using density functional theory (DFT), we present an investigation of the properties of nickel (Ni) doped MoS_2 monolayer nanosheets. We studied three possible methods for introducing Ni atoms into the MoS_2nanosheet. First, we examined the effect of Ni atom decoration on the properties of the pristine MoS_2nanosheet.Our calculations revealed that Ni exhibits chemisorption above the Mo atom with an adsorption energy of -3.44 eV, and the band gap has reduced from 1.743 eV in pristine MoS_2 to 1.528 eV. Next, we investigated two possible substitutional doping methods to replace Mo or S vacancies with Ni atoms. Energy considerations showed that the S vacancy substitution is exothermic and most favorable. The Mo vacancy substitution was endothermic and dramatically changed MoS_2's electronic properties, transforming it from a semiconductor to a conductor. The S vacancy substitution reduced the band gap to 0.682 eV. Nevertheless, all band gaps were direct, as was the case for the pristine MoS_2 monolayer. Density of states (DOS) analysis revealed that the 3d orbital states of the Ni atom exhibit significant hybridization with the d states of the nearest Mo atoms. It is primarily responsible for the change in electronic properties.

Keywords: Monolayer MoS_2, DFT, Density of states, Doping, Band structure, Electronic properties

1 Introduction

The successful isolation of two-dimensional (2D) graphene[1] sparked significant interest in 2D materials due to their unique physical and chemical properties[2]. 2D materials show physical phenomena that are quite different from their three-dimensional (3D) counterparts due to reduced dimensionality and symmetry[3]. The electronic industry is moving toward miniaturization, and there is a great demand for alternative materials that may replace traditional semiconductor devices that seem to have reached a dead-end while entering the nanoscale era[4]. However, the absence of a band gap in graphene restricts its applicability in electronic applications, prompting various methods to be explored for incorporating a band gap to enhance its usability[5].

Semiconducting Transition Metal Dichalcogenides (TMDs) are an emerging class of materials due to their excellent mechanical, electrical, optical, and transport properties, as well as their relative ease of stacking to create new heterostructures with wide applications in electronic technologies.[6]. The general chemical formula of TMD may be expressed as MX_2, where M represents transition metals from groups 4-10 of the periodic table of elements. At the same time, X comes from the chalcogenide elements group 16, like H, S, Se, and Te[7].The bulk form of TMDs is composed of X-M-X layers stacked via van der Waals (vdW) forces. The bulk TMDs exhibit a broad range of electrical properties, spanning from semiconductors (such as MoS_2 and $MoSe_2$) to semimetals (like WTe_2 and VS_2), and including metals like TaS_2 and NbS_2[8]. Many researchers have found that the physical and chemical properties of these materials depend on the number of layers. While bulk MoS_2 exhibits an indirect bandgap of 1.2 eV, its monolayer possesses a direct band gap of 1.8 eV[9].

Among (TMDCs), 2D Molybdenum Disulfide (MoS_2) particularly has received significant attention from researchers due to its moderate band gap and favorable optical properties that make it suitable for electronics and optoelectronics applications[10]. It is beneficial for gas sensing[11], catalysis, and solid lubrication due to its thermal stability, large surface area, and high surface activity[12,13]. Due to their broadband sensitivity and fast response time, this monolayer is used in Field Effect Transistor (FET) technology as a subthreshold swing transistor and

*Corresponding author: E-mail:i.hassan@uokirkuk.edu.iq

photodetector[14]. It is ideal for thin-film transistors due to its simple fabrication process, which yields high production at a low cost[15]. The ammonia gas sensing properties of heteroatoms doped 2D MoS_2 have been reported[16]. One of the significant advantages of MoS_2 is its small metal-semiconductor interface contact resistance compared to silicon devices. This means that MoS_2 may be used in 1 nm gate transistors with high efficiency and excellent switching characteristics[17,18]. $MoS_2$is promising for many electronic fields, such as microwave and terahertz applications[19,20]. It has been reported that many molecules, such as SO_2, H_2O, and formaldehyde, have a good tendency to be adsorbed on metal-doped MoS_2 nanosheets[21] Since MoS_2 has no biological interaction and is safe for injection in human bodies. Some biosensing applications have also been reported, such as DNA, cancer[22], and coronavirus detection[9]. Different fabrication methods have been used for MoS_2monolayer production, such as wet exfoliation, chemical vapor deposition, and atomic layer deposition[23].

Understanding the electronic properties of both pristine and distorted 2D MoS_2 is crucial for developing electronic devices, gas sensors, energy storage systems, and other applications. This is mainly achieved by investigating the band structure and density of states of the material. Several methods can be employed to modulate and engineer the physical properties of 2D nanosheets, including doping or decorating with other elemental species, introducing vacancy defects, applying strain, or incorporating transition metal atoms into the monolayer[24,25]. In 2D materials, adsorption and vacancy substitution doping with atoms is expected to induce substantial changes because it can significantly perturb the uniform two-dimensional array[26].

Transition metal (TM) doped MoS_2 is gaining attention due to the strong interactions between TM and MoS_2, which result in a significant number of free electrons. This makes TM-doped MoS_2 a promising candidate for applications in sensing technologies, catalytic processes, and energy storage, where incorporation of different TMs enables the tuning of the electronic structure, which results in optimizing the material's properties to meet specific application needs[27]. Among the transition metals, the 3d transition metal nickel (Ni) is an inexpensive metal that possesses a high redox potential ($Ni^{2+}/Ni^{3+}/Ni^{4}$) and significant electronegativity. Its activation effects on the graphene surface for hydrogen storage applications have been investigated in a DFT study. The results showed a remarkable enhancement in hydrogen storage capacity within an acceptable adsorption energy[28].

The present work provides insight into the structural and electronic properties of pristine, Ni-decorated, and doped MoS_2 monolayers. We expect that the interaction with the MoS_2 surface is significant, utilizing its wide range of charge states, regardless of the initial oxidation state of the Ni atoms. We employed Density Functional Theory (DFT), a first-principles perspective, to investigate the structural, electronic band structure, and density of states of the samples. We expect it may interfere with the saturated Mo-S bond on the non-edge state surface of MoS_2, leading to modifications in the electronic structure. This modification facilitates the effective attachment of other molecules to the Ni-adsorbed and doped MoS_2 surface. Consequently, this process is expected to significantly enhance the adsorption capacity, rendering it a more effective gas sensor and a promising material for molecular hydrogen storage.

2 Calculation Methodology

All calculations of this work have been performed using the first principles method DFT implemented in CASTEP code[29].The contribution of exchange-correlation (XC) to the total energy was treated using the generalized gradient approximation (GGA) and parameterized using Perdew-Burke-Ernzerhof (PBE) XC potentials[30]. GGA-PBE is a nonlocal gradient-corrected functional that is supposed to give a good description of the gradient expansion over a wide range of densely packed solids[31]. It is widely used for investigating electronic properties because its description depends on electron density and its gradient, offering a reasonable cost-to-accuracy ratio compared to the local density approximation. The effect of spin polarization was ignored throughout this work.

The geometry optimization calculations using the GGA-PBE method were performed with the following settings: energy convergence accuracy of 10^{-5} eV/atom, maximum stress of 0.05 GPa, and maximum displacement of 0.001 Å. The BFGS minimizer was selected because of its ability to perform cell optimization[32]. It is well known that DFT-based GGA functionals underestimate the energy band gap[33]. Nevertheless, this method works well for calculating overall energy and optimizing the equilibrium structures of solids[34].

All calculations, including geometry optimization and electronic structure properties (band structure and density of states), were performed using a (3x3x1) supercell, which consists of 9 Mo atoms and 18 S atoms, as illustrated in Fig. 1. The distance between neighboring layers was set to 30 Å to prohibit any interaction between layers. We used a (5x5x1) grid for Mokhorst-Pack sampling of the Brillouin Zone (BZ)[35].The self-consistent field tolerance was set to 10^{-6} eV. We selected the on-the-fly generation (OTFG) ultra soft pseudo potentials for electronic properties calculations. This option allows calculations to be performed with lower energy cutoffs. OTFG produces potential that is consistent between solid-state and pseudo-atom calculations, as they use the same XC functionals[29].

We analyzed the adsorption of Ni atom on the monolayer MoS_2surface depending on the adsorption energy (E_{ads}), also denoted as formation energy, which is defined as:

$$E_{ads} = E_{Ni@MoS2} - E_{Ni} - E_{MoS2} \quad \ldots (1)$$

where: E_{MoS2}, $E_{Ni@MoS2}$, and E_{Ni} are the total energies of the pristine MoS_2 sheet, the Ni-decorated MoS_2 sheet, and the free Ni atom, respectively. The negative values of adsorption energy indicate that the adsorption process is exothermic and stable.

The substitutional doping process of the MoS_2 monolayer with Ni atoms was discussed by analyzing the difference in formation energy (ΔE_f) of the doped MoS_2monolayerwitha Niatom replacing either a Mo or an S atom to find out which process is more favorable, which is defined as:

$$\Delta E_f = E_{MoS2-Ni} - E_{MoS2} - E_{Ni} + E_{(Mo\ or\ S)} \quad \ldots (2)$$

were, $E_{Ni-MoS2}$The total energy of Ni-dopedMoS_2nanosheet.This analysis will clarify whether the formation of the three structures studied is exothermic, which is represented by a negative value (ΔE_f negative), or endothermic, indicated by a positive value(ΔE_f positive). An exothermic reaction releases energy into the surroundings, resulting in a decrease in internal energy, while an endothermic reaction absorbs energy, leading to an increase in internal energy. Understanding the thermodynamic nature of these structures is crucial for predicting their stability and behavior under various conditions

3 Results and Discussion

3.1 Properties of Pristine Monolayer MoS_2

This work started by constructing the MoS_2 monolayer from its bulk structure—the bulk MoS_2 forms layered structures of the S-Mo-S units, which are covalently bonded. The neighboring layers are held together by the weak vdW force, which binds the adjacent S-S layers. The Mo and S atoms are arranged in a hexagonal structure such that each Mo is located at the center of a trigonal prism and surrounded by six S neighbors. In other words, the MoS_2 monolayer has a tri-layer structure composed of the Mo layer sandwiched between two S layers. The crystal structure of monolayer MoS_2 belongs to hexagonal symmetry with a space symmetry group that is P-6M2. The primitive cell includes a single Mo atom and two S atoms. The (3×3×1) supercell was chosen to study the doping and decoration of Ni atoms on the

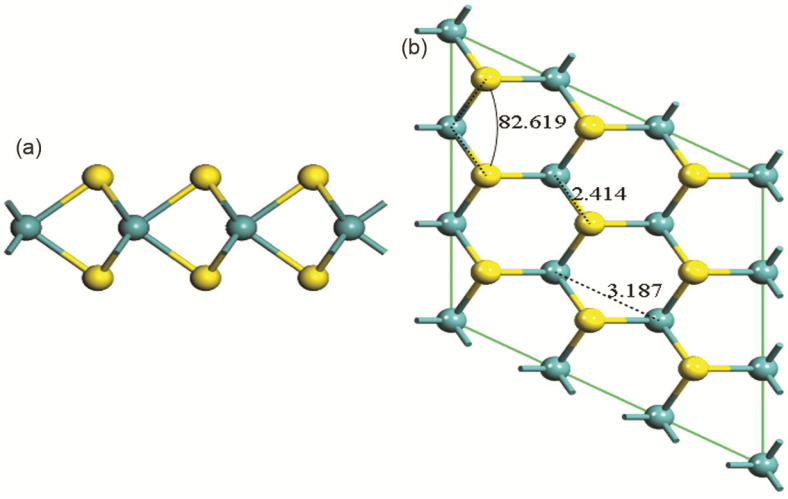

Fig. 1 — (a) Side; and (b) Top views of geometrically optimized structures of a 3x3x1 supercell of pristine MoS_2 (Color scheme: Mo, green; S, yellow)

MoS2 single layer, which is composed of nine Mo atoms and eighteen S atoms. The vacuum between layers was set to 30 Å to avoid interactions between periodic layers. Figure 1 shows the side and top views of the geometrically optimized monolayer MoS_2. The final optimized monolayer pristine MoS_2 lattice constant is calculated to be 3.187Å, which is in good agreement with other reported results[36]. The angle of S-Mo-S is calculated to be 82.619 °, and the Mo-S bond length is calculated to be 2.414 Å. All of these are in good agreement with the parameters reported in previous studies[37]. The thickness of the monolayer and the distance between two adjacent Mo atoms were calculated to be 3.125Å and 3.187 Å, respectively, which is also in agreement with the reported results[38].

The band structure of pristine $MoS_2$was calculated and plotted in Fig. 2a along high symmetry directions. Typically, the Γ→M→K→ Γ path direction points in the irreducible Brillouin zone are considered for hexagonal crystal structures. The band structure of the bulk MoS_2 shows an indirect band gap of 1.2 eV between the Γ point at the top of the valence band and the halfway point between the Γ and K points at the bottom of the conduction band[39]. In monolayer MoS_2, this indirect band gap becomes wider than the direct band gap located at the K point. The calculated direct energy band gap (E_g) at the K point was 1.743 eV. This is attributed to the fact that as the number of layers decreases, the band gap increases due to the quantum confinement effect. Our results went very well with other results that have been published[40,41]. It is well known that the GGA-PBE functional, which is commonly used, underestimates the energy band gap. Hybrid functionals, such as HSE03, which offer higher accuracy comparable to experimental values, may be used as an alternative. The results are shown in Table 1.

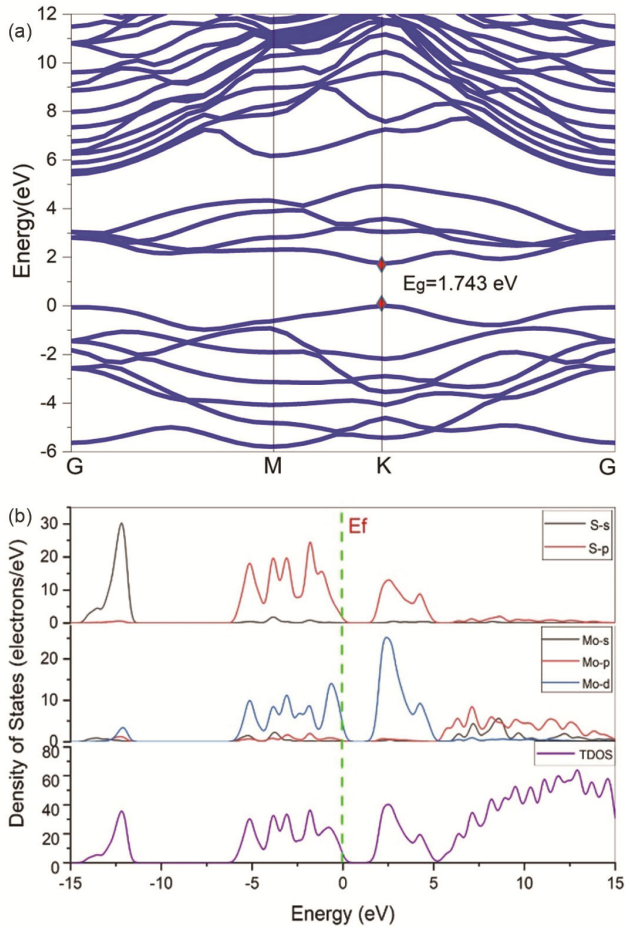

Fig. 2 — (a) Electronic band structures showing the direct band gap of the pristine monolayer (MoS_2); and (b) Total density of states (TDOS) and partial density of states (PDOS) for pristine MoS_2

To perform additional analysis on the electronic characteristics of pristine and Ni-doped MoS_2 monolayers, the density of states for each structure under study has been calculated and plotted. The density of states (DOS) refers to the number of available energy states per unit energy per unit volume. The total density of states (TDOS) refers to the total energy states; on the other hand, the partial or projected density of states (PDOS) reflects the contribution from the individual orbitals of different atoms in the material to the total DOS. Figure 2b shows the plots of the calculated TDOS and PDOS of pristine MoS_2. The most significant contribution to the DOS comes from the p and d orbitals of S and Mo atoms. Respectively. The strong hybridization is evident between the 3d orbital of the Mo and the 2p orbital of the S.

In CASTEP, all energies are calculated relative to the top of the valence band and considered as the Fermi level. It is observed that the edge of the valence DOS is extending slightly beyond the Fermi Level. This contributed to applying Gaussian smearing to the energy levels of each band in the DOS calculation and

Table 1 — The energy band gap of pristine MoS_2 compared with other published results.

Ref.	XC Functional	Program	Band gap(eV)	Gap type
Present Study	GGA-PBE	CASTEP	1.743	Direct
[40]	GGA-PBE	VASP	1.693	Direct
[41]	GGA-PBE	SIESTA	1.760	Direct
[42]	……	Practical	2.340	Direct

then sampling using a histogram. This approach cannot capture the sharp features in the DOS; nevertheless, it may represent the overall shape of the DOS with a limited number of k-points.

3.2 Properties of Monolayer MoS_2 Decorated with Ni Atom

The Ni-decorated monolayer MoS_2 sheet is constructed by attaching a Ni atom to the surface of pure MoS_2 and performing geometry optimization. The adsorption energy of Ni on MoS_2 is dependent on the adsorption site. There are four possible sites for the adsorption of a Ni atom to be considered (a) above the Mo atomic site, (b) above the S atomic site, (c) above the center of the hexagonal ring composed of three S atoms, and (d) above the Mo-S bond, as shown in Fig. 3.

The final position of the adsorbed Ni atom was settled above the Mo atom location (B) after geometry optimization in all cases, or the adsorption energy calculated using Eq 1 was positive, indicating an unstable or less favorable adsorption strategy. This finding aligns strongly with the conclusions drawn by other researchers, thereby reinforcing the validity of our results[41]. The final optimized structure is shown in Fig. 3 (e) and 3 (f). As shown in Fig. 3 (e), the decorated Ni atoms were found to remain above the MoS_2 monolayer plane due to the large atomic radius of 1.49 Å. At the same time, the neighboring S atoms shifted from their original positions to alleviate the additional stress caused by the decorated Ni. The S-Mo bond length in the neighboring Ni atom is 2.517 Å, while the Ni-S bond length is 2.12 Å. This is attributed to the higher electronegativity difference between the Ni and S atoms, which attracts the nearest S atoms and stretches the neighboring S-Mo bonds. It is observed that the S-Mo bond lengths away from the decoration site are very close to those of pristine MoS_2, indicating that the Ni atom only locally affects its near neighbors.

Our results indicate that the $\boldsymbol{E}_{ads}$ value for the Ni atom is -3.44 eV, suggesting that the Ni atom is preferentially chemisorbed onto the Mo atom. This value agrees very well with other published results[41]. The negative value of the adsorption energy $\boldsymbol{E}_{ads}$ means that the Ni atom decoration on $MoS_2$is an exothermic reaction.

Surface functionalizing through adsorption is a practical approach; nevertheless, it has a relatively weak influence on band structure or electronic properties in our case, as shown in Fig. 4 (a). The dopant states are seen to exist in considerable density in the formerly forbidden gap of the pristine MoS_2, as shown in Fig. 4 (b). The interaction between a single adsorbed Ni atom and MoS_2 can also be revealed from their electron-state density. The *Ni-3d* orbital contributed to the impurity states introduced around the Fermi level. The newly calculated energy band gap is narrowed to E_g=1.528 eV, which is in good agreement with the value of 1.54 eV reported by Barzegar *et. al*[41] The hybridization

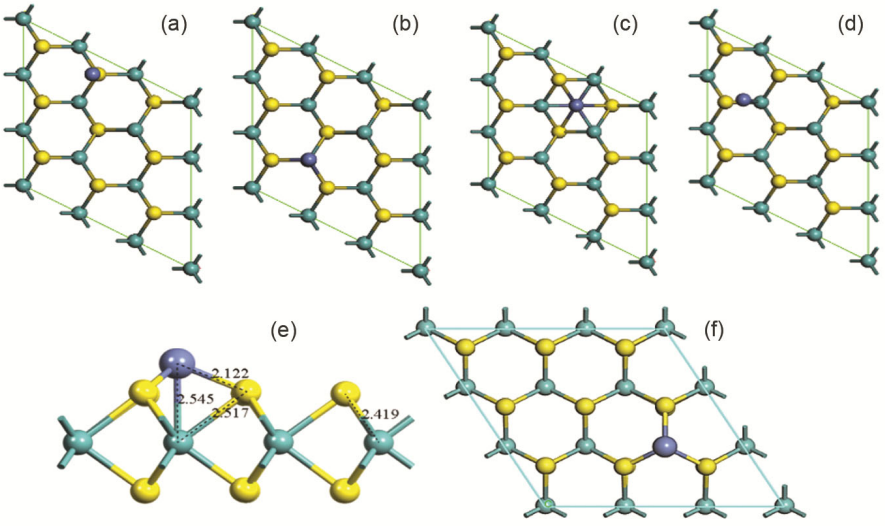

Fig. 3 — The possible absorption sites of the Ni atom (blue) (a) above the S atom, (b) above the Mo atom (the favorite position), (c) above the center of the hexagonal ring, (d) above the Mo-S bond; and (e, f) side and top view respectively of the final optimized geometry (Ni blue)

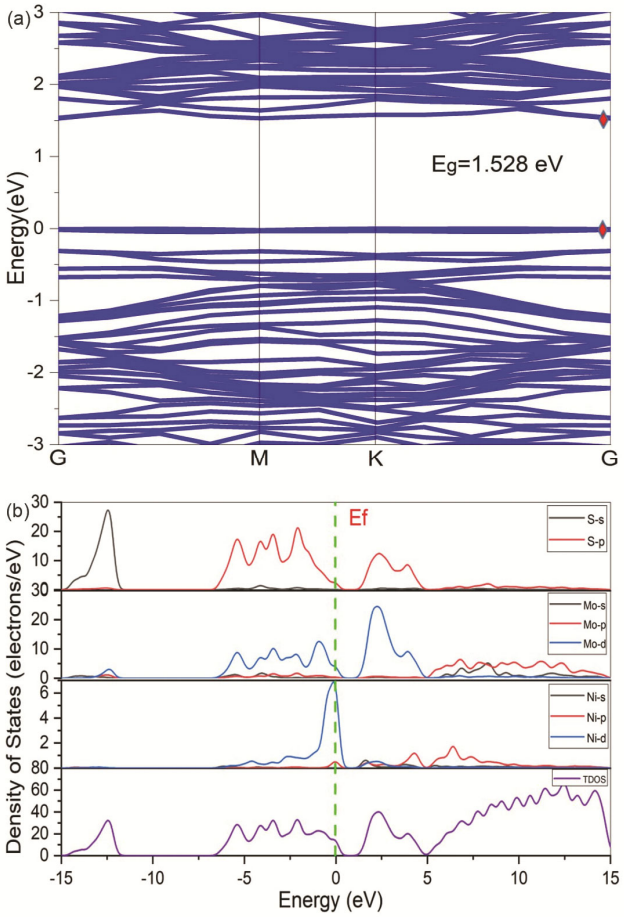

Fig. 4 — (a) Band structures of Ni-decorated MoS_2 monolayer; and (b) Density of states of Ni-decorated monolayer MoS_2

around the Fermi level is now due to the *d* or bitals of both Mo and Ni atoms, as may be noticed from the PDOS plot in Fig. 4 (b).

3.3 Properties of the Ni-doped MoS_2Monolayer

In 2D semiconductors, substitutional doping, which involves replacing a host atom with another atom, has been successfully employed as an effective means to modify their electronic and optical properties[43]. Substitutional doping is often more stable and more efficient in tuning the bandgap. This can be achieved by replacing the host MoS_2 atoms with Ni atoms. There are two possibilities in the doping case first, to replace the Mo atom, or second, to replace the S atom. Both structures were geometrically optimized, and their electronic properties were subsequently studied. The final structures are shown in Fig. 5(a) and 5(b). Initially, we considered the electronic structure of a single substitutional Ni for Mo in a 3x3 supercell with 2.8% Ni doping concentration.

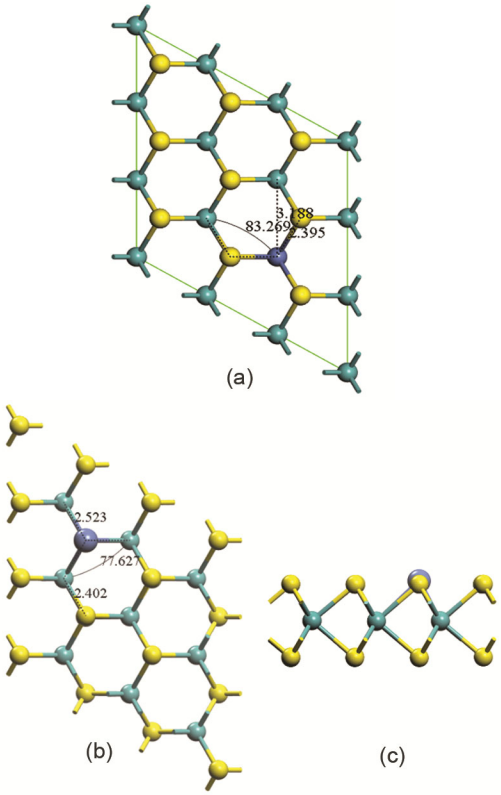

Fig. 5 – geometrically optimized substitutional Ni-doped monolayer MoS_2. a) Mo atom substituted; (b) S atom substituted (Top view); and (c) S atom substituted (Side view)

Figure 6 (a) shows the energy band structure of the Ni-doped MoS_2 monolayer by substituting the Mo atom with the Ni atom. We conclude from the band structure that the energy gap disappears and the valence and conduction bands overlap. This means that the monolayer MoS_2 nanosheet was changed from a semiconductor to a conductor. However, the formation energy calculations using Eq.(2) revealed that this type of doping is endothermic and unfavorable. The density of states of the MoS_2 nanosheet is shown in Fig. 6 (b) after substituting one Mo atom with a Ni atom. It is noticed that the 3dorbital of the Ni atom is mainly behind the overlapping between the valence and conduction bands.

The other possibility is the substitution of a Ni atom into the S vacancy. This type of doping was realized by the Laser-Assisted Reaction selective doping approach[43]. Fig. 5 (b) and 5 (c) show the final optimized geometrical structure of Ni replacement of S vacancy. The Ni-Mo bond length is calculated to be 2.524 Å. It is noticed from Fig. 5 (c) that the dopant atom Ni is moved a small distance above the sulfur plane. Figure 7 (a) shows the band

structure after replacing the S vacancy with the Ni atom. It reveals that the band gap is still direct and narrowed to 0.682 eV. This value is in good agreement with other reported results[44]. The introduced energy states from the 3d orbital are responsible for reducing the energy band gap value. It overlaps with the 2p states of the S atoms, as well as the 3d states of the Mo atoms. Figure 7 (b) shows the DOS of Ni atom substitution into the S vacancy.

It is noticed from the band structures after Ni incorporation that the top of the valence band becomes flatter. The shape of the valence band graph is closely related to the effective mass of charge carriers in semiconducting materials. A flatter curvature indicates a greater effective mass for charge carriers, meaning they are massive and more challenging to move.

The analysis of the 3x3 super lattice parameters shows that Ni-decorated and Mo vacancy-doped by Ni changed by only 1.1% and 0.6%, respectively. However, there are considerable local changes in bond lengths around the decoration or doping site. On the other hand, the S vacancy-doped sample's super lattice parameter changed by 4.9%. This is attributed to the lower electro negativity difference between Ni and Mo atoms (0.25) compared to the electronegativity difference between S and Mo atoms (0.42). This results in a longer Ni-S bond length of 2.523 Å and shorter Mo-S bond lengths of 2.402 Å. However, no phase transition is detected, and the hexagonal symmetry stays consistent.

The formation energy, as determined by Eq.(2) has been closely examined to assess the stability and thermodynamic favorability of the two potential doping scenarios. The findings are summarized in Table 2. The

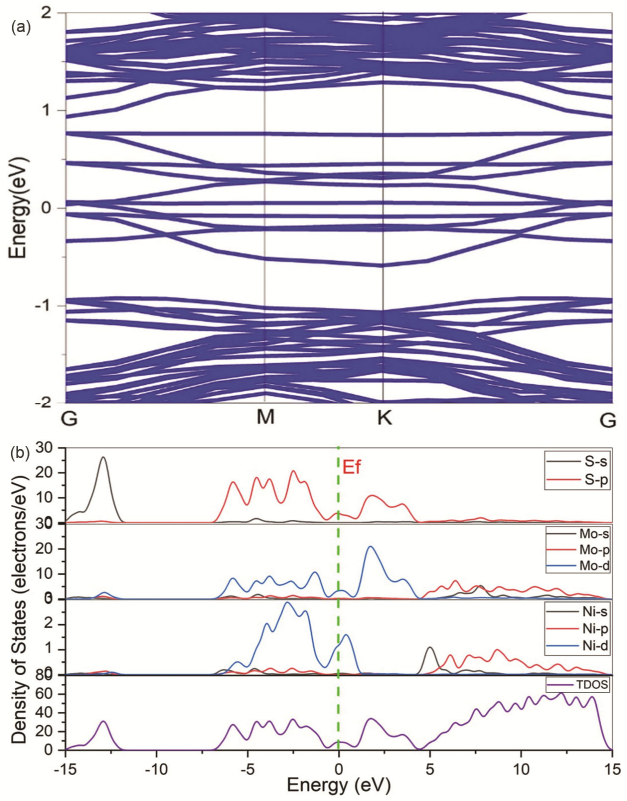

Fig. 6 — (a) Electronic band structure for Mo vacancies substituted Ni-MoS_2; and (b) Density of states for Mo vacancies substituted Ni-MoS_2

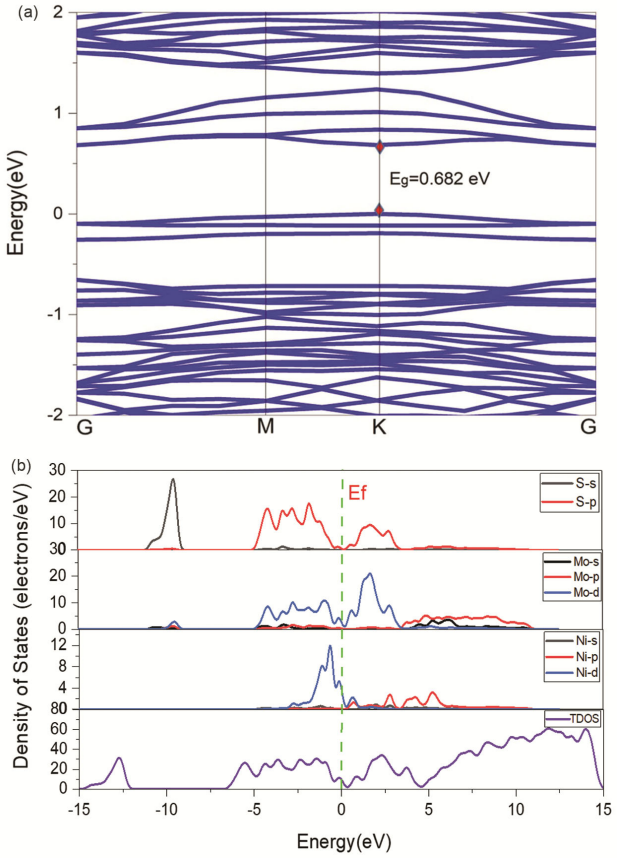

Fig. 7 — (a) Electronic band structure for S vacancies substituted Ni-MoS_2; and (b) Density of states for S vacancies substituted Ni-MoS_2

Table 2 — Summarizing the lattice parameters, formation energy, and band gap of the investigated samples

Sample	Super Lattice parameter (Å)	Formation energy (eV)	Band gap (eV)
Pristine MoS_2	9.559	---	1.743
Ni decorated	9.579	-3.443	1.528
S vacancy doped	9.511	-4.206	0.682
Mo vacancy doped	9.564	22.916	conductor

analysis reveals that the process of replacing sulfur (S) vacancies is substantially more advantageous and exothermic relative to the substitution of molybdenum (Mo) atoms. The latter process is characterized as endothermic and exhibits lower stability compared to the pristine MoS_2 structure. This conclusion is supported by the corresponding total energy calculations, which indicate that the substitution of Mo not only increases the energy of the system but also destabilizes the overall structure, making the S vacancy replacement a far more energetically favorable option for doping in MoS_2.

4 Conclusion

Two-dimensional MoS_2 monolayer sheets decorated and doped with Ni atoms have been explored using DFT calculations. We observed considerable changes in the band structure and density of states, especially in substitutional doping cases. The band structure calculations of pristine MoS_2 confirmed a direct band gap with an energy value of 1.743 eV. The adsorbed Ni atom was attached to the surface of the MoS_2 sheet above the Mo atom with a chemisorption energy of -3.44 eV, while the direct band gap decreased to 1.528 eV. We examined vacancy substitutional doping for both Mo and S sites. The formation energy values revealed that the S vacancy substitution is stable, more favorable, and exothermic. On the other hand, the Mo substitutional doping was endothermic and unfavorable. It transformed the monolayer semiconductor MoS_2 into a conductor by introducing the 3d orbital states of the Ni atom, which caused the overlap of the conduction and valence bands. The more stable substitutional doping of S vacancies with Ni atoms reduced the band gap to 0.682 eV, which is also attributed to the 3d orbital states of the Ni atoms. It is observed that Ni incorporation flattens the valence band, which means a larger effective mass of charge carriers. The calculated formation energy suggests that the Ni atom is firmly bonded to S vacancies, primarily due to the significant hybridization between the 3d states of the do pant Ni and its nearest Mo atoms. No phase transition is detected, and the hexagonal symmetry stays consistent in all the samples investigated. A local bond length change has been noticed around the Ni incorporation sites. Almost no change in lattice parameters has been observed except for the S vacancy substitutional doping, where a shortening of 4.9% has resulted.

References

1 Geim A K & Novoselov K S, *Nature Mater,* 6 (2007) 183.
2 Bian R, Li C, Liu Q, Cao G, Fu Q, Meng P, Zhou J, Liu F & Liu Z, *Natl Sci Rev,* 9 (2022).
3 Shanmugam V, Mensah R A, Babu K, Gawusu S, Chanda A, Tu Y, Neisiany R E, Försth M, Sas G, Das O, Shanmugam V, Mensah R A, Försth M, Sas G, Das O, Babu K, Gawusu S, Tu Y & Neisiany R E, *Part & Part Syst Charact,* 39 (2022) 2200031.
4 Tian J, Wang Q, Huang X, Tang J, Chu Y, Wang S, Shen C, Zhao Y, Li N, Liu J, Ji Y, Huang B, Peng Y, Yang R, Yang W, Watanabe K, Taniguchi T, Bai X, Shi D *et al*, *Nano Lett,* 23 (2023) 2764.
5 Hassan I Z & Ali E M, *Turk J Comp Math Edu,* 12 (2021) 1269.
6 Wei H, Gui Y, Kang J, Wang W & Tang C, *Nanomater,* 8 (2018) 646.
7 Islam M R, Rana M M & Islam A S M J, *Int Confer Electr Electron Eng,* (2017) 1.
8 Yamusa S A, Shaari A, Alsaif N A M, AlsalamahI M, Isah I & Rekik N, *ACS Omega,* 7 (2022) 45719.
9 Thomas N, Mathew S, Nair K M, Dowd K O, Forouzandeh P, Goswami A, Mc Granaghan G & Pillai S C, *Mater Today Sustain,*13 (2021).
10 Rai D P, Vu T V, Laref A, Joshi H & Patra P K, *Chem Phys,* 538 (2020).
11 Kuş E, Altındemir G, Bostan Y K, Taşaltın C, Erol A, Wang Y & Sarcan F *Nanomater,* 14 (2024) 633.
12 Hussain S, Akbar K, Vikraman D, Shehzad M A, Jung S, Seo Y & Jung J, *RSC Adv,* 5 (2015) 15374.
13 Chen Y M, Yu X Y, Li Z, Paik U & Lou X W, *Sci Adv,* 2 (2016).
14 Zou J, Cai Z, Lai Y, Tan J, Zhang R, Feng S, Wang G, Lin J, Liu B & Cheng H M, *ACS Nano,*15 (2021) 7340.
15 Yoo G, Lee S, Yoo B, Han C, Kim S & Oh M S, *IEEE Electron Device Lett,* 36 (2015) 1215.
16 Gber T E, Louis H, Owen A E, Etinwa B E, Benjamin I, Asogwa F C, Orosun M M & Eno E A, *RSC Adv,* 12 (2022) 25992.
17 Desai S B, Madhvapathy S R, Sachid A B, Llinas J P, Wang Q, Ahn G H, Pitner G, Kim M J, Bokor J, Hu C, Wong H S P & Javey A, *Sci,* 354 (2016) 99.
18 Wu F, Tian H, Shen Y, Hou Z, Ren J, Gou G, SunY, Yang Y & Ren T L, *Nature,* 603 (2022) 259.
19 Wei H, Gui Y, Kang J, Wang W & Tang C, *Nanomater,* 8 (2018) 646.
20 Saliba M, Atanas J P, Howayek T M & Habchi R, *Nanoscale Adv,* 5 (2023) 6787.
21 Li H, Fu L, He C, Huo J, Yang H, Xie T, Zhao G & Dong G, *Front Chem*, 8 (2021) 605311.
22 Chhetri D, Pokhrel S, Chettri B, Karki P, Chettri P, Das S K & Sharma B, *Proceedings of 5th International Conference on Devices for Integrated Circuit*, (2023) 542.
23 Samy O, Zeng S, Birowosuto M D & El Moutaouakil A, *Crystals*, 11 (2021) 355.
24 Hussain A, Asif Q U A, Nabi A G, Asim H & Rafique H M, *Phys Scr*, 98 (2023) 025807.
25 Phuc H V, Hieu N N, Hoi B D, Hieu N V, Thu T V, Hung N M, Ilyasov V V, Poklonski N A & Nguyen C V, *J Electron Mater*, 47 (2018) 730.
26 Hassan I Z & Ali E M, *Turk J Comp Math Edu*, 12 (2021) 1269.

27 Boakye D, Martin H, Labik L K, Britwum A, Nunoo O A, Elloh V W, Kwakye-Awuah B, Yaya A & Abavare E K K, *Physica Status Solidi B*, 260 (2023) 2200337.

28 Zainalabdeen Hassan I & Hawas Khorsheed A, *J Edu Sci*, 30 (2020) 11.

29 Clark S J, Segall M D, Pickard C J, Hasnip P J, Probert M I J, Refson K & Payne M C, *Zeitschrift Fur Kristallographie,* 220 (2005) 567.

30 Perdew J P, Burke K & Ernzerhof M, *Phys Rev Lett*, 77 (1996) 3865.

31 Perdew J P, Ruzsinszky A, Csonka G I, Vydrov O A, Scuseria G E, ConstantinL A, Zhou X & Burke K*, Phys Rev Lett,* 100 (2008) 136406.

32 Pfrommer B G, Côté M, Louie S G & Cohen M L, *J Comput Phys*, 131 (1997) 233.

33 HassanI Z, Kadhem H A, Hakim A & Mohammed S, *Ind J Pure Appl Phys*, 61 (2023) 840.

34 Pelá R R, Caetano C, Marques M, FerreiraL G, Furthmüller J & Teles L K, *Appl Phys Lett*, 98 (2011) 151907.

35 Wang Y, Wisesa P, Balasubramanian A, Dwaraknath S & Mueller T, *Comput Mater Sci*, 187 (2021) 110100.

36 Ulian G & Valdrè G, *J Appl Crystallogr*, 56 (2023) 611.

37 Deng X, Liang X, Ng S P & Wu C M L, *Appl Surf Sci*, 484 (2019) 1244.

38 Wang J, Zhou Q, Lu Z, Gui Y & Zeng W, *Physica E Low Dimens Syst Nanostruct*, 113 (2019) 72.

39 Yamusa S A, Shaari A, Alsaif N A M, AlsalamahI M, Isah I & Rekik N, *ACS Omega*, 7 (2022) 45719.

40 Chen C Y, Li Y & Chuang M H, *Nanomater*, 13 (2022) 68.

41 Barzegar M, Berahman M & Asgari R, *J Comput Electron,* 18 (2019) 826.

42 Sah R K, Tang H, Shahi C, Ruzsinszky A & Perdew J P, *Phys Rev B*, 110 (2024) 144109.

43 Kim E, Ko C, Kim K, Chen Y, Suh J, Ryu S G, Wu K, Meng X, Suslu A, Tongay S, Wu J & Grigoropoulos C P, *Adv Mater,* 28 (2016) 341.

44 Wei H, Gui Y, Kang J, Wang W & Tang C, *Nanomater,* 8 (2018).